1 # Seismicity characterization of oceanic earthquakes in the Mexican
2 # territory

4 **Quetzalcoatl Rodríguez-Pérez**[1,2,*]**, Víctor Hugo Márquez-Ramírez**[2]**, and Francisco Ramón**
5 **Zúñiga**[2]

7 [1] Consejo Nacional de Ciencia y Tecnología, Dirección Adjunta de Desarrollo Científico, Mexico
8 [2] Centro de Geociencias, Universidad Nacional Autónoma de México, Juriquilla, Querétaro, Mexico
9
10 **Correspondence:** Quetzalcoatl Rodríguez-Pérez (quetza@geociencias.unam.mx)

11 Víctor Hugo Márquez-Ramírez (marvh@geociencias.unam.mx)

12 Francisco Ramón Zúñiga (ramon@geociencias.unam.mx)

1   **Abstract.** We analyzed the seismicity of oceanic earthquakes in the Pacific oceanic regime of Mexico.

2   We used data from the earthquake catalogs of the Mexican National Service (SSN), and the

3   International Seismological Center (ISC) from 1967 to 2017. Events were classified into two different

4   categories: intraplate oceanic (INT), and transform faults zone and mid-ocean ridges events (TF-MOR),

5   respectively. For each category, we determined statistical characteristics such as magnitude frequency

6   distributions, the aftershocks decay rate, the non-extensivity parameters, and the regional stress field.

7   We obtained b-values of 1.17, and 0.82 for the INT, and TF-MOR events, respectively. TF-MOR

8   events also exhibit local b-value variations in the range of $0.72 - 1.30$. TF-MOR events follow a

9   tapered Gutenberg-Richter distribution. We also obtained a p-value of 0.67 for the 1 May 1997 (M_w =

10   6.9) earthquake. By analyzing the non-extensivity parameters, we obtained similar q-values in the

11   range of 1.39-1.60 for both types of earthquakes. On the other hand, the parameter a showed a clear

12   differentiation, being higher for TF-MOR events than for INT events. This implies that more energy is

13   released for TF-MOR events. Stress orientations are in agreement with geodynamical models for

14   transform faults zone and mid-ocean ridges zones. In the case of intraplate seismicity, stresses are

15   mostly related to a normal fault regime.

18   **1 Introduction**

20   Mid-ocean ridges and transform faults zones are two of the main morphological features of oceanic

21   environments. Most of the oceanic earthquakes take place in areas close to the active spreading ridges

22   where the seismogenic zone is narrow. For this reason, long ruptures are often required to produce large

23   oceanic earthquakes. The rupture process of oceanic events is still poorly understood. Previous studies

24   showed that these types of events have peculiar characteristics. For example, estimates of seismic

1   coupling for oceanic transform faults indicate that about three-fourths of the accumulated moment are

2   released aseismically (Abercrombie and Ekström, 2003; Boettcher and Jordan, 2004). Early studies

3   also showed that some oceanic events exhibit slow slip ruptures (Kanamori and Stewart, 1976; Okal

4   and Stewart, 1992; McGuire et al., 1996). On the other hand, others proposed that the slow ruptures

5   may be explained as numerical artifacts generated by the inversion procedures (e.g., Abercrombie and

6   Ekström 2001; 2003). Several oceanic strike-slip events were reported as being energy deficient at

7   high-frequencies (Beroza and Jordan, 1990; Stein and Pelayo, 1991; Ihmlé and Jordan, 1994), or

8   having high apparent stresses (Choy and Boatwright, 1995; Choy and McGarr, 2002). On another front,

9   oceanic earthquakes also occur as intraplate events, but to a lesser extent.

11 From the statistical perspective, previous studies showed that the magnitudes of the major events in the

12 mid-oceanic ridges and transform faults zones are relatively small ($6.0 \leq M_w \leq 7.2$) compared to

13 continental events. The b-value in oceanic environments showed significant variability. For example,

14 Tolstoy et al. (2001) reported high b-values ($b \sim 1.5$) in the Gakkel Ridge associated with volcanic

15 activity. In the Southwest Indian Ridge, Läderach (2011) found b-values of about 1.28. Bohnenstiehl et

16 al. (2008) quantified the b-value in the East Pacific Rise, obtaining estimations in the range of $1.10 < b$

17 < 2.50. Global studies have also shown that the mid-ocean ridge transform seismicity follows a tapered

18 frequency-moment distribution (Kagan and Jackson, 2000; Boettcher and McGuire, 2009). Cowie et al.

19 (1993) studied the seismic coupling on mid-ocean ridges. They found that fast-spreading ridges (≥ 9.0

20 cm/yr) are weakly coupled. On the contrary, slow-spreading ridges (≤ 4.0 cm/yr) are strongly coupled

21 (Cowie et al., 1993). For oceanic ridge transform faults, the seismic coupling coefficient (χ) mainly

22 varies from 0.01 to 0.97 with an abnormal reported value of 1.79 (Table B1 of Boettcher and Jordan,

23 2004). This unusual high value of χ reported by Boettcher and Jordan (2004) was excluded from their

24 analysis. The seismic coupling coefficient is in the range of $0 \leq \chi \leq 1$. A value of $\chi = 1$ represents a full

1 seismic coupling. In Mexico, oceanic earthquakes have been poorly studied. There are no systematic

2 studies on their statistical characteristics. In this article, we characterized the oceanic seismicity in

3 Mexico. We determined the orientation of the principal stresses, the *b*- and *p*-values, and the non-

4 extensivity parameters. The results may help to understand the ocean tectonics, particularly in Mexico.

6 **2 Tectonic Setting**

8 The Pacific oceanic regime of Mexico is an active area exhibiting ongoing tectonic plate interactions.

9 These interactions involve the Cocos (CO), the Pacific (PA), the Rivera (RI), and the North American

10 (NA) plates (Fig. 1). The Gulf of California and the Middle America Trench (MAT) are separated by

11 the Tamayo Fracture Zone (TFZ) (Fig. 1). The convergence rate between the RI, and NA plates

12 decreases northward along the MAT (averaging about 2–3 cm/yr in the RI plate, which is slower than

13 the adjacent CO plate, about 5–7 cm/yr) (NUVEL-1a model, DeMets et al., 1994) (Fig. 1). Sea-floor

14 spreading takes place along the northernmost segment of the East Pacific Rise in the Cocos, and Rivera

15 segments (EPR-CS, and EPR-RS, respectively) (Fig. 1). In the EPR-RS, the spreading rates range from

16 5.3 cm/year at the northern to 7.3 cm/year at the southern end of the rise (Bandy, 1992) (Fig. 1). The

17 spreading rates at the EPR-CS are: 7.0 cm/yr near the Rivera Fracture Zone (RFZ); 8.2 cm/yr near the

18 Orozco Fracture Zone (OFZ); 10.1 cm/yr near the Clipperton Fracture Zone (CFZ); and 10.7 cm/yr

19 near the Siqueiros Fracture Zone (SFZ) based on the NUVEL-1a model (DeMets et al., 1994; Pockalny

20 et al., 1997) (Fig. 1). The Rivera Transform (RT) is a left transform fault with fast slipping (~ 7.0

21 cm/year) (Bandy et al., 2011) (Fig. 1). Due to these differences in subduction, and spreading rates, and

22 convergence direction of the RI and CO plates, complex seismicity patterns are generated in this

23 region. In the last century, some intermediate-size earthquakes have taken place in the Pacific oceanic

24 regime of Mexico such as: the 14 January 1899 ($M = 7.0$) (DNA project); the 17 December 1905 ($M_w =$

1   7.0) (Pacheco and Sykes, 1992); the 10 April 1906 (M_w = 7.1) (Pacheco and Sykes, 1992); the 31

2   October 1909 (M_s = 6.9) (ISC catalog); the 31 May 1910 (M_s = 7.0) (ISC catalog); the 29 October 1911

3   (M_s = 6.8) (ISC catalog); the 16 November 1925 (M_s = 7.0) (Abe, 1981); the 28 May 1936 (M_s = 6.8)

4   (ISC catalog); the 30 June 1945 (M_s = 6.8) (ISC catalog); the 04 December 1948 (M_s = 6.9) (ISC

5   catalog); the 29 September 1950 (M_s = 7.0) (Abe, 1981); and the 1 May 1997 (M_w = 6.9) (Global CMT

6   catalog) earthquakes (Table 1 and Fig. 2).

8   **3 Data and Methods**

10 **3.1 Data**

11 We used earthquake catalogs of the Mexican National Service (SSN), and the International

12 Seismological Center (ISC) from 1967 to 2017. Events without magnitude were excluded from our

13 analysis. Reported magnitudes (based on superficial, M_s; body, m_b; and coda, M_c; waves) were

14 converted to moment magnitude (M_w). The SSN reports M_w for events in Mexico. For the case of the

15 ISC events, M_s, and m_b were converted to M_w using the scaling relationships of Scordilis (2006). We

16 classified the seismic events into two different categories: 1) intraplate oceanic events (INT, red dots in

17 Fig. 2), and 2) transform faults zone and mid-ocean ridges events (TF-MOR, green dots in Fig. 2). The

18 INT catalog consists of 177 events with magnitudes in the range of 2.9 - 6.0. The TF-MOR catalog is

19 made of 2074 earthquakes with magnitudes in the following interval 2.7 - 6.9. We also used the Global

20 CMT focal mechanism catalog (Dziewonski et al., 1981; Ekström et al., 2012) with solutions from

21 1976 to 2017. For the stress analysis, the focal mechanism catalog was divided into 6 sub-catalogs

22 shown in Fig. 8 (R1 to R6).

1 **3.2 Methods**

2 **3.2.1 Moment/magnitude earthquake distributions**

3 The Gutenberg-Richter law describes the occurrence of earthquakes as a function of their magnitude

4 (Ishimoto and Iida, 1939; Gutenberg and Richter, 1944). Mathematically, this law is expressed by the

5 following equation: $log_{10} N(M) = a - bM$, where N(M) is the cumulative number of earthquakes with a

6 magnitude larger than a given magnitude limit (M), the constant b (or b-value) describes the slope of

7 the size distribution and the constant a is proportional to the seismic productivity. The b-value

8 describes the distribution of small to large earthquakes in a sample. The b-value is considered to be a

9 feature for a given tectonic environment (e.g., Scholz, 1968; Wyss, 1973; Smith, 1981; Wiemer and

10 Benoit, 1996). In several tectonic environments, b is close to 1 (Utsu, 1961), but many factors affect it.

11 Among them, high thermal gradients and rock heterogeneity (Mogi, 1962; Warren and Latham, 1970)

12 increases the b-values. On the contrary, increments in effective and shear stresses (Scholz, 1968; Wyss,

13 1973; Urbancic et al., 1992) reduce the b-value. The b-value differs between unrelated fault zones

14 (Wesnousky, 1994; Schorlemmer et al., 2005), but also for specific space and time periods (Nuannin et

15 al., 2012). Schorlemmer et al. (2005) found a global dependence of the b-value on focal mechanism,

16 which was corroborated at a regional level by Rodríguez-Pérez and Zúñiga (2018). According to those

17 authors, the highest b-values correspond to normal-faulting events, followed by strike-slip, and thrust

18 earthquakes, respectively. We estimated the b-value by the maximum likelihood formula of Aki (1965),

19 and the completeness magnitude (M_c) with the maximum curvature method (Wiemer and Wyss, 2000).

20 We used the ZMAP software package (Wiemer, 2001) for estimating the b-value, and M_c.

22 As reported by previous authors, seismicity on the mid-ocean transform faults is better represented by a

23 tapered frequency moment distribution (e.g., Boettcher and McGuire, 2009). This distribution has the

24 following form (Kagan, 1997, 1999; Kagan and Jackson, 2000; Kagan and Schoenberg, 2001; Vere-

1 Jones et al., 2001):

$$N(M)=N_o\left(\frac{M_o}{M}\right)^{\beta}\exp\left(\frac{M_o-M}{M_m}\right) \ , \tag{1}$$

5 where β is one of the parameters to determine ($\beta = (2/3)b$, where b is the b-value), N_0 is the cumulative

6 earthquake number over a completeness threshold seismic moment (M_0), and M_m is the maximum

7 expected moment. We analyzed if this frequency distribution is suitable for describing the seismicity of

8 oceanic events in Mexico. In order to calculate the tapered Gutenberg-Richter distribution, we used the

9 Matlab function Get_GR_parameters.m developed by Olive (2016). The tapered Gutenberg-Richter

10 moment distribution is fitted by mens of a least-squares inversion following Frohlich (2007).

12 **3.2.2 Temporal distribution of aftershocks**

13 The frequency distribution of the decrement of earthquake aftershocks is described by the modified

14 Omori's law (Utsu, 1961; Utsu et al., 1995) as:

$$R(t)=\frac{k}{(t+c)^p} \ , \tag{2}$$

18 where $R(t)$ is the rate of occurrence of aftershocks within a given magnitude range, t is the time interval

19 from the mainshock, k is the productivity of the aftershock sequence, p is the power-law exponent (p-

20 value), and c is the time delay before the onset of the power-law aftershock decay rate. Variations of p-

21 values exist for different tectonic regimes, and each aftershock sequence. As before, we used the

22 ZMAP software package (Wiemer, 2001) for estimating the p-value of the aftershock sequence of the 1

1 May 1997 earthquake ($M_w = 6.9$).

3.2.3 Fragment-asperity model

4 Sotolongo-Costa and Posadas (2004) introduced the fragment-asperity model to describe the

5 earthquake dynamics in a Tsallis entropy non-extensive framework (Tsallis, 1988). This model takes

6 into consideration the irregular surfaces of two fault planes in contact and the rock fragments of

7 different shape and sizes that fill the space between them. According to this model, earthquakes are

8 triggered by the interaction along the fault planes of these rock fragments. Considering that large

9 fragments are more difficult to release than small ones, the resulting energy is assumed to be

10 proportional to the volume of the fragment (Telesca, 2010). Silva et al. (2006) improved the model and

11 found a scaling law between the released energy (ε), and the size of asperity fragments (r) by the

12 following proportional factor: $\varepsilon \propto r^3$. The non-extensive statistics is used to describe the volumetric

13 distribution function of the fragments. A parameter that represents the proportion between ε and r is

14 introduced. This parameter is known as the a-value or parameter a (Silva et al., 2006; Telesca, 2010).

15 The parameter a is defined using a volumetric distribution function of the fragments applying the

16 maximum entropy principle for the Tsallis entropy (for details in the mathematical expressions see

17 Silva et al., 2006; Telesca, 2010). The magnitude cumulative distribution function becomes:

19 $$\log_{10}(\text{N>M}) = \log_{10}(N) + \left(\frac{2-q}{1-q}\right)\log_{10}\left[1 - \left(\frac{1-q}{2-q}\right)\left(\frac{10^K}{a^{2/3}}\right)\right] \quad , \tag{3}$$

21 where N is the total number of earthquakes; $N\ (>M)$ represents the number of events with magnitude

22 larger than M; a is a proportionality parameter between ε and r, and; q is the non-extensivity parameter.

23 K is defined as $K = 2M$ (Silva et al., 2006), or $K = M$ (Telesca, 2011). The magnitude (M) is related to

1   ε by the following relation: $M = 1/3 \log(\varepsilon)$ (Silva et al., 2006). Telesca (2011) considered that the

2   relation between ε and M is given by $M = 2/3 \log(\varepsilon)$ (Telesca, 2011). None of both models are preferred

3   over the other. We used both models in order to quantify the variability of the non-extensive

4   parameters. According to Telesca (2010), the physical meaning of the q-parameter consists in that it

5   provides information about the scale of interactions. It means that if q is close to 1, the physical state is

6   close to the equilibrium. As a result, few earthquakes are expected. On the other hand, as q rises, the

7   physical state goes away from the equilibrium state, this implies that the fault planes are able to

8   generate more earthquakes, thus resulting in an increment in the seismic activity (Telesca, 2009; 2011).

9   The physical meaning of the a-value lies in the fact that it provides a measure of the energy density. It

10 means that the a-value is large if the energy released is large (Telesca, 2011). For example, high a-

11 values are expected when the events with the highest magnitude take place. Previous studies have

12 shown that the q-value ranges mainly from 1.50 to 1.70 (Vilar et al., 2007; Vallianatos, 2009;

13 Rodríguez-Pérez and Zúñiga, 2017; among others). We obtained the a and q parameters by minimizing

14 the root mean square error (RMS) with the Nelder-Mead method (Nelder and Mead, 1965).

16 **3.2.5 Stress Inversion**

17 In order to study the regional stress field for oceanic earthquakes, we performed stress tensor inversion

18 from focal mechanisms reported in the Global CMT catalog (Dziewonski et al., 1981; Ekström et al.,

19 2012) with the iterative joint inversion developed by Vavryčuk (2014). From the stress inversion, we

20 obtained the orientation of the principal stress axes σ_1, σ_2, and σ_3 (where $\sigma_1 \geq \sigma_2 \geq \sigma_3$), and the stress

21 ratio R. We now briefly explain each method. The first method (the iterative joint inversion), provides

22 an accurate estimation of R and stress orientations (Vavryčuk, 2014). In this method, the ratio is defined

23 as $R = (\sigma_1 - \sigma_2)/(\sigma_1 - \sigma_3)$ (Gephart and Forsyth, 1984). A fault instability constraint is applied, and the

24 fault is identified with that nodal plane which is more unstable, and thus more susceptible to faulting

1 (Vavryčuk, 2014). By incorporating a fault instability constraint into the inversion, an iterative

2 procedure is imposed. The uncertainties are determined as the differences between the inverted results

3 considering noisy data (Vavryčuk, 2014). The stress inversion was carried out with the

4 STRESSINVERSE software developed by Vavryčuk (2014). The maximum horizontal stress (SH_{max})

5 was calculated using the formulation of Lund and Townend (2007). The stress inversion was performed

6 for each of the six different regions shown in Fig. 7.

4 Results

10 The b-value for the INT events is 1.17 ± 0.1 with a $M_c = 4.4$ (Fig. 3). The cumulative seismic moment

11 for these events is $\sum M_0 = 3.57$ x 10^{25} Nm. For the INT events, the non-extensive parameters are: $q =$

12 1.60, and $a = 6.69$ x10^{12}; and $q = 1.39$, and $a = 2.27$ x10^6 for the Silva's and Telesca's models,

13 respectively (Fig. 3). For INT events, both models have similar curve fittings (Fig. 3). In the case of the

14 TF-MOR events, the b-value is 0.82 ± 0.02 with a $M_c = 4.2$ (Fig. 4a). The cumulative seismic moment

15 for these events is $\sum M_0 = 12.76$ x 10^{26} Nm. TF-MOR events also exhibit local b-value variations in the

16 range of $0.72 - 1.30$ (Fig. 4b) for each of the subregions R1 to R5 (Table 2). Results for TF-MOR

17 events also show that the tapered Gutenberg-Richter distribution fits better the earthquake data than the

18 common Gutenberg-Richter distribution (Fig. 5a). The tapered Gutenberg-Richter distribution was

19 fitted with the following parameters: $\beta = 0.64$, and the estimated magnitude of $M_m = 6.7$ (Fig. 5a). The

20 regions that have the worst fitting with a Gutenberg-Richter distribution are subregions R1 and R2

21 (Figs. 4b and 5b). In the case of the TF-MOR events, the non-extensive parameters are: $q = 1.60$, and a

22 $= 3.22$ x10^{13}; and $q = 1.41$, and $a = 3.55$ x10^6 for the Silva's and Telesca's models, respectively (Fig. 6).

23 TF-MOR events also exhibit local a and q-value variations for each of the subregions R1 to R5 (Table

24 2, and Fig. 6). For TF-MOR events, the best fit was obtained with Telesca's model (Fig. 6). By

1 analyzing the aftershock sequence of the 1 May 1997 earthquake (M_w = 6.9), we found a *p*-value of

2 0.67 ± 0.33 (Table 3). The magnitude of the largest aftershock of the 1997 event is M_w = 5.3 (Table 3).

4 The region R1 is composed of strike-slip (70.3%), strike-slip with normal and reverse components

5 (21.6%, and 5.4%, respectively), and normal-faulting (2.7%) focal mechanisms (Fig. 7b). In region R2,

6 there are strike-slip (82.4%), and strike-slip with normal and reverse components earthquakes (9.5 %,

7 and 8.1 %, respectively) (Fig. 7b). Region R3 is composed of strike-slip (62.5%), strike-slip with

8 normal component (25%), normal-faulting with strike-slip component (6.3%), and reverse events

9 (6.3%)(Fig. 7b). In region R4, there are strike-slip (70.8%), strike-slip with normal and reverse

10 components (8.3%, and 16.7 %, respectively), and reverse events (4.2%)(Fig. 7b). In region R5, strike-

11 slip (53%), strike-slip with normal and reverse components(23.5%, and 17.6%, respectively), and

12 reverse (5.9%) earthquakes take place (Fig. 7b). For the case of region R6, earthquakes exhibit a

13 normal (83.3%) and normal-faulting with strike-slip component (16.7%) focal mechanisms (Fig. 7b).

15 Table 4 summarizes the results from the stress inversion. The region R6 is only dominated by N and N-

16 SS earthquakes (Fig. 8). In regions R4 and R5, stress results showed moderate similarities. The

17 differences in these regions may also be related to the variability of the focal mechanisms (here we

18 have SS, SS-N, SS-R, and to lesser extent R events) (Fig. 8). Variations are very significant in regions

19 R1 to R3 (spatially in σ_2) (Table 4). These regions also showed different types of events: SS, SS-N, SS-

20 R for R1; SS, SS-N, SS-R for R2; and SS, SS-N, N-SS, R for R3 (Fig. 8). In the case of the East Pacific

21 Rise Rivera segment (region R1), σ_2 is almost vertical, and SH_{max} is ~ 170° suggesting a strike-slip

22 regime (Table 4). For the case of the Rivera Transform (region R2), σ_2 is quasi vertical, and the SH_{max} is

23 157° suggesting a strike-slip regime (Table 4). In region R3, σ_2 is almost vertical, and the SH_{max} is also

24 157° suggesting a strike-slip regime (Table 4). For the region R4, σ_2 is 76, and the SH_{max} is 22°

1   suggesting a strike-slip regime (Table 4). In R5, σ_2 is from 69º, and the SH_{max} is 120º suggesting a

2   strike-slip regime (Table 4). In R6, the principal axes are related to a normal fault regime. σ_1 is almost

3   vertical, and the SH_{max} is ~ 45º (Table 4).

5   **5 Discussion**

7   One of the main problems for studying oceanic seismicity is that the epicenters are located far from

8   most of the recording stations in mainland Mexico. This has a direct effect on the earthquake

9   magnitude distributions (M_c and b-value). Our results show that M_c is 4.4 and 4.2 for INT and TF-MOR

10   events, respectively. M_c for oceanic events is higher than reported M_c for the subduction zone, and

11   continental regions of Mexico. The magnitude completeness for oceanic earthquakes differs for

12   different parts of the World, but in most cases it is in the range of 4.0 – 5.0 on average considering most

13   of the global catalogs. Several microseismic surveys have been conducted in different oceanic

14   environments (e.g., Smith et al., 2003; Simão et al., 2010; McGuire et al., 2012; among others). As a

15   result of these studies, precise hypocenter locations and earthquake distributions with a broader

16   magnitude range were obtained. Thus lower M_c is reported for studies based on microseismic surveys.

17   For example, in the Mid-Atlantic Ridge, M_c ~ 3.0 with several smaller events (M_w < 2.5) were reported

18   (Bohnenstiehl et al., 2002; Smith et al., 2002, and 2003).

20   The location uncertainty plays an important role when earthquakes are assigned to an intraplate or a

21   mid-ocean ridge/transform fault environment. For example, some studies reported that for faults

22   located at 4S on the EPR, teleseismic locations could be off as much as 50 km (McGuire, 2008;

23   Wolfson-Schwehr, 2014). As a consequence, some TF-MOR events are probably classified as INT

24   events, and vice-versa (for example, epicenters in color in Fig. 2). Some events located in the Tamayo

1 Fracture Zone close to the Rivera subduction zone may also be mislabeled. This mislocation effect

2 introduces uncertainties on the estimation of the statistical parameters. In order to have precise

3 locations an avoid mislocation, ocean-bottom seismometers along the Mexican coast are needed. Being

4 aware of this, one should avoid over-interpretation of the results. Local monitoring of oceanic events

5 represents an improvement of more than an order of magnitude relative to the regional, and teleseismic

6 detection levels. For this reason, it is difficult to establish a direct comparison with our results with

7 those from studies based on microseismic surveys.

9 Previous studies also showed that the seismicity on oceanic transform faults that connect mid-ocean

10 ridges are thermally controlled (Abercrombie and Ekström, 2001; Boettcher et al., 2007). Regarding

11 the thermal effect on the seismogenic zone. It is essential to mention that faults along the middle and

12 southern segments of the EPR are shorter and faster-slipping. The faster slip rates and shorter fault

13 lengths result in narrower seismogenic zones because the thermal structure is shallow. On the other

14 hand, the Rivera Transform is longer, and has a slower slip rate, resulting in a wider seismogenic zone.

15 However, heat is not the only factor that regulates seismicity because the largest events break a small

16 part of the rupture areas predicted by thermal models (Boettcher and Jordan, 2004; Roland et al., 2010).

17 Thus most slip occurs without producing large earthquakes (Boettcher and Jordan, 2004; Roland et al.,

18 2010). This can explain the occurrence of a few events with $M > 6.5$ in the Rivera Transform.

19 According to McGuire et al. (2012), the apparent lack of large events on mid-ocean ridge transform

20 faults may also be related to the heterogeneity of materials on the fault plane. The maximum magnitude

21 for transform fault events on the East Pacific Rise (in the latitude interval of $3° < Lat < 5°$) is about 6.5

22 (McGuire et al., 2005). On the other hand, earthquakes in the Rivera Transform and on the northern

23 segment of the East Pacific Rise (in Mexico) have relative larger magnitudes ($M > 6.8$) based on

24 reported seismicity in different catalogs (Fig. 1). This highlights a differentiation between the mid-and

1   southern and northern segments of the East Pacific Rise.

3   Earthquake statistical studies showed that large oceanic events in transform faults, fracture zones, and

4   intraplate regions release low energy levels in their aftershock sequences (Houston et al., 1993;

5   Boettcher and Jordan, 2001; Antolik et al., 2006). Boettcher et al. (2012) found that earthquakes on

6   transform faults have an order of magnitude fewer aftershocks than intraplate events. According to

7   some authors, a low aftershock-to-mainshock energy ratio indicates an efficient rupture or complete

8   stress drop in the mainshock presupposing a weak fault (Hwang and Kanamori, 1992; Velasco et al.,

9   2000). Many factors can affect the aftershock productivity, for example the age of the lithosphere and

10   the heat flux have a direct influence on the rock strength (Antolik et al., 2006), thus, explaining the low

11   energy release in the aftershock sequence of oceanic events. The observed low aftershock energy seems

12   to be a common feature of oceanic earthquakes (Antolik et al., 2006). In this regard, we studied the 1

13   May 1997 ($M_w = 6.9$) strike-slip event in the Rivera Transform and its largest aftershock ($M_w = 5.3$). By

14   considering the energy magnitude as $\log E = 1.5\ M_w + 11.8$, we obtain that the energy of the mainshock

15   is 1.41 x 10^{22} ergs, and the energy of the largest aftershock is 5.62 x 10^{19} ergs resulting in an aftershock-

16   to-mainshock energy ratio of 0.003. This value is considered as low and representative of strike-slip

17   events, as shown by the comparison with the results reported by Velasco et al. (2000). A similar

18   analysis comes from Båth's law by considering the magnitude difference between the mainshock, and

19   the largest aftershock. We determined that the magnitude difference for the 1997 event is 1.6, which is

20   higher than the theoretical value of 1.2. Both magnitude difference and the aftershock-to-mainshock

21   energy ratio showed large scatter (e.g., Velasco et al., 2000; Utsu, 2002), and results ought to be taken

22   with caution.

24   The aftershock decay rate is the product of the strain relaxation around the rupture plane. Aftershock

1   studies have shown that oceanic ridges are prone to have *p*-values greater than one due to the high

2   temperature of the oceanic crust resulting in rapid strain release (Kisslinger, 1996; Rabinowitz and

3   Steinberg, 1998; Klein et al., 2006). According to previous studies, extremely high *p*-values ($p > 2$),

4   and short aftershock durations are related to high temperatures (Bohnenstiehl et al., 2002; Simão et al.,

5   2010), and/or migration of hydrothermal fluids (Goslin et al., 2005). Oceanic strike-slip events seem to

6   have lower *p*-values than mid-ocean ridges events. For example, Bohnenstiehl et al. (2004) found a *p*-

7   value of 0.95 for the 15 July 2003 ($M_w = 7.6$) central Indian Ridge strike-slip event. For the Siqueiros,

8   Discovery, and western Blanco transforms, the *p*-value varies from 0.94 to 1.29 (Bohnenstiehl et al.,

9   2002). Davis and Frohlich (1991) determined a *p*-value of 0.928 ± 0.024 for the combined ridge and

10 transform environments. We found a *p*-value of 0.67 ± 0.33 for the 1 May 1997 ($M_w = 6.9$) strike-slip

11 event in the Rivera transform. Our results fall within the range of global studies that showed that the *p*-

12 value varies from 0.6 – 2.5 (Utsu et al., 1995). We also reported a *c* close to 0 for the aftershock

13 sequence of the 1 May 1997 ($M_w = 6.9$) (Table 3). Shcherbakov et al. (2004) found that the parameter *c*

14 of the Omori's law decreases as the magnitude of events considered increases. According to them, this

15 observation is due to the effect of an undercount of small aftershocks in short time periods. This

16 provides an explanation for our result of $c \sim 0$ because of the limited magnitude detection reported in

17 the regional and global catalogs used.

19 Estimations of *b*-value at different scales (local, regional, or global) have shown a significant departure

20 from the theoretical result of $b \sim 1$. In the case of the oceanic events, previous studies showed large

21 fluctuations in the *b*-values. For example, Tolstoy et al. (2001) reported *b*-values of about 1.5

22 associated with volcanic activity in the Gakkel Ridge. Läderach (2011) reported *b*-values of 1.28 in the

23 Southwest Indian Ridge. In a global study, Molchan et al. (1997) estimated the *b*-value for mid-ocean,

24 and transform zones, obtaining values of the following interval 0.97 – 1.47. Along the East Pacific Rise

1   (in the latitude interval of 5ºN < Lat < 9.90ºN), *b*-value fluctuates from 1.10 to 2.50 (Bohnenstiehl et

2   al., 2008). Bohnenstiehl et al. (2008) determined the *b*-value of 9000 earthquakes with magnitudes in

3   the range of -1.5 – 1.0. The study of Bohnenstiehl et al. (2008) took place in the southern part of our

4   study zone, but their results are based on microearthquakes occurring in 1 year. Due to this overlap, we

5   compare their results with our results for region R5. For R5, we obtained a *b*-value of 0.94 with a M_c of

6   4.2. Bohnenstiehl et al. (2008) found that the *b*-value approaches 2.5 at very shallow depths (< 0.3 km)

7   (with M_c = -1.3). At depths of 0.5 to 1.5 km, the *b*-values drops to a value of 1.10 (with M_c = -0.4).

8   According to Bohnenstiehl et al. (2008) at very shallow depths, the uppermost oceanic crust is

9   structurally heterogeneous because of the extrusion of lava, and the repeated emplacement of sheeted

10   dikes. As a consequence, there is a large proportion of small versus large earthquakes resulting in high

11   *b*-values. The *b*-values decreases with depth due to the decreasing heterogeneity, and/or changes in

12   ambient stress levels. Considering that events in our catalog for R5 occur at a different depth interval,

13   and assuming the decreasing heterogeneity, less low magnitude events are expected (reducing the *b*-

14   value). Another explanation for the differences between our results and the results of Bohnenstiehl et

15   al. (2008) is that the magnitude ranges of the earthquake catalogs are extremely different. This

16   highlights how the *b*-value is affected by magnitude completeness.

18   Statistical studies suggested that *β*-value mainly takes values between 0.60 and 0.70 for a global range

19   (Kagan, 2002). Bird et al. (2002) studied the tapered Gutenberg-Richter distribution for spreading

20   ridges and oceanic transform faults based on global data obtaining a *β*-value of about 0.67 for both

21   types of events. Bird et al. (2002) reported corner magnitudes (M_m in Eq. (1)) varies from 5.8 to 6.6 –

22   7.1 for mid-ocean ridge and transform faults, respectively. Bird et al. (2002) also found a dependence

23   of *β*-value on the relative plate velocity. According to them, the *β*-value is higher (with M_m = 7.1) when

24   the velocity is < 36 mm/yr than when the velocity is > 67 mm/yr (with M_m = 6.6) for spreading ridges,

1   and oceanic transform faults, respectively. These observations are in agreement with our estimate of $\beta =$

2   0.64, and M_m of 6.6 for oceanic earthquakes in Mexico (Figure 5). For intraplate events, we obtained a

3   $\beta > 0.70$. According to Kagan (2010), β-values > 0.70 may be related to the mix of earthquake

4   populations with different maximum magnitudes (M_m). In the case of intraplate events, we associated

5   the somewhat high β-values with the mix of some intraplate, and mid-ocean- transform events. This

6   could be related to incorrect hypocenter locations due to the difficulty of precisely locating oceanic

7   events by the landbased networks.

9   The seismicity models based on non-extensivity consider the interaction of two irregular fault surfaces

10 (asperities), and rock fragments filling them. However, these models differ in their assumption of how

11 energy is stored in the fragments, and the asperities. This difference is expressed through the constant

12 a, which represents the proportionality between the released energy E, and the fragment size r. This

13 explains the difference in a parameter between Telesca's and Silva's models (Fig. 5). Both models

14 showed that a for TF-MOR is higher than a for the INT events (Fig. 5). This implies that more energy

15 is released for TF-MOR earthquakes. On the other hand, the q-value indicates if the physical state of a

16 seismic area moves away from equilibrium. The physical state is at equilibrium when q is equal to 1,

17 and as q increases, the system is in an instability state in which a more significant amount of seismic

18 energy is released. Individually, we found higher q-values for TF-MOR events than for INT events

19 (Fig. 5), meaning that TF-MOR events are farther from the equilibrium than INT events. The results

20 showed a better fitting for cumulative distribution functions using the Telesca model for TF-MOR and

21 each of the regions (Fig. 6). In regions R1-R5, our results showed that q varies from 1.31 to 1.52, and

22 from 1.57 to 1.63 using the Telesca's and Silva's models, respectively. In the case of subduction zones,

23 the q-value can vary from 1.35 to 1.70. For example, in the Hellenic Subduction Zone, q is in the range

24 of 1.35 - 1.55 (Papadakis et al., 2013); in the Mexican subduction zone, Valverde-Esparza et al. (2012)

1 found that q varies from 1.63 to 1.70. Thus, our results conform to values obtained in regional studies.

3 Focal mechanisms provide useful information about the structure, and settings of faults, and can

4 describe the crustal stress field in which earthquakes take place. Our analysis is limited because we

5 only used focal mechanisms based on teleseismic data. Reported focal mechanisms confirm Sykes's

6 model for mid-ocean ridges (Sykes, 1967), where events in transform zones tend to have strike-slip

7 mechanisms, while ridge crest events have mainly normal faults. The teleseismic detection threshold

8 for oceanic events in the East Pacific Rise is dependent on the region of the EPR. For example,

9 Riedesel et al. (1982) report a magnitude detection threshold in the range of $4.0 - 5.0$. For the

10 Quebrada, Discovery, and Gofar faults, the CMT catalog is only complete to $M_\mathrm{W} = 5.4$. (McGuire,

11 2008; Wolfson-Schwehr et al., 2014). Another limitation of our study is that we combine different types

12 of earthquakes into a single region, resulting in inaccurate estimations of the stress state for that

13 specific region. Under these circumstances, our study provides information on the stress field of major

14 structures or the stress associated with the dominant types of earthquake.

16 In oceanic environments, the largest magnitude events along transform fault or intraplate earthquakes

17 usually show strike-slip mechanisms (Wiens and Stein, 1984; Kawasaki et al., 1985). In the adjacent

18 areas to the oceanic ridges where the oceanic lithosphere is young, Wiens and Stein (1984) report a

19 large variety of focal mechanisms and stress orientations. For example, in the East Pacific Rise, in the

20 Mexican territory, Wiens and Stein (1984) reported thrust and normal mechanism solutions for near

21 ridge intraplate seismicity. This explains the strike-slip with normal components, as well as thrust

22 events in regions R3, R4, and R5 (Fig. 7). In R3, and R4 (Fig. 7), the maximum horizontal axes

23 (compression) of thrust events show a preferred orientation perpendicular to the spreading direction.

24 On the other hand, in region R5 (Fig. 7), the compression axes, showed a weak preferred alignment

1   with respect to the spreading direction. In the Rivera transform, focal mechanisms showed right lateral

2   strike-slip motion implying oblique horizontal stresses (Fig. 7). Although most of the events in the

3   Rivera transform (R2 in Fig. 7) are strike-slip events, some events with unusual mechanisms have been

4   reported (normal faulting events) (Wolfe et al., 1993). Normal faulting events may be related to

5   extensional offsets or internal deformation of the Rivera plate (Wolfe et al., 1993).

7   **6 Conclusions**

9   We analyzed the seismicity of oceanic events in the Pacific oceanic regime of Mexico. Oceanic

10   earthquakes were classified into two different categories: intraplate oceanic (INT), and transform faults

11   zone and mid-ocean ridges events (TF-MOR), respectively. We conducted a stress state estimation for

12   the different regions. Because of combination of different types of earthquakes into the regions, our

13   results only provide information on the stress field of major structures or the stress associated with the

14   dominant types of earthquakes. It is important to be aware of this limitation in order to avoid an over-

15   interpretation of the results. TF-MOR events have strike-slip, strike-slip with normal and reverse

16   components, normal and normal-faulting with strike-slip component, and reverse focal mechanisms.

17   On the other hand, INT events have only normal, and normal-faulting with strike-slip component focal

18   mechanisms. The stress field from INT, and TF-MOR events agree with global studies. Regarding the

19   aftershock productivity, we found that the aftershock decay rate of the 1 May 1997 ($M_w = 6.9$) strike-

20   slip event in the Rivera transform is also consistent with oceanic p-value estimations. Although the

21   limitation of the catalogs used, our results provided a general insight into the seismicity of oceanic

22   environments. The main problem is the location uncertainty and mislabelling of the earthquakes. The b-

23   value for INT events (1.17) is higher than that for TF-MOR events (0.82). Our b-values estimations are

24   in agreement with other regional studies but differ from b-value estimates based on microseismicity

1   studies. Our b-value estimates for mid-ocean ridge/transform fault environments are lower ($0.72 < b <$

2   1.30) than those derived from microseismicity studies ($1.1 < b < 2.5$). Our results also showed that TF-

3   MOR events mostly follow a tapered Gutenberg-Richter distribution.

5   From the non-extensivity analysis, we observed that TF-MOR events are farther from the equilibrium

6   than INT events. Thus high q-values take place in mid-ocean ridges, and transform faults zones. This

7   means that mid-ocean ridge and transform faults are able to produce more seismicity. Low q-values are

8   also reported during relatively quiet periods, characterized mainly by the occurrence of small

9   magnitude events. This can be an explanation for the low q-values of regions R1 and R5. Our results

10   also showed that a-values are higher for TF-MOR events than for INT events using both models. This

11   implies that more earthquakes with larger magnitude occur (or more energy is released) in mid-ocean

12   ridge/transform fault environments than in an oceanic continental environment. Telesca's model fits

13   better with the cumulative magnitude distribution functions making a better option to study the oceanic

14   seismicity in Mexico.
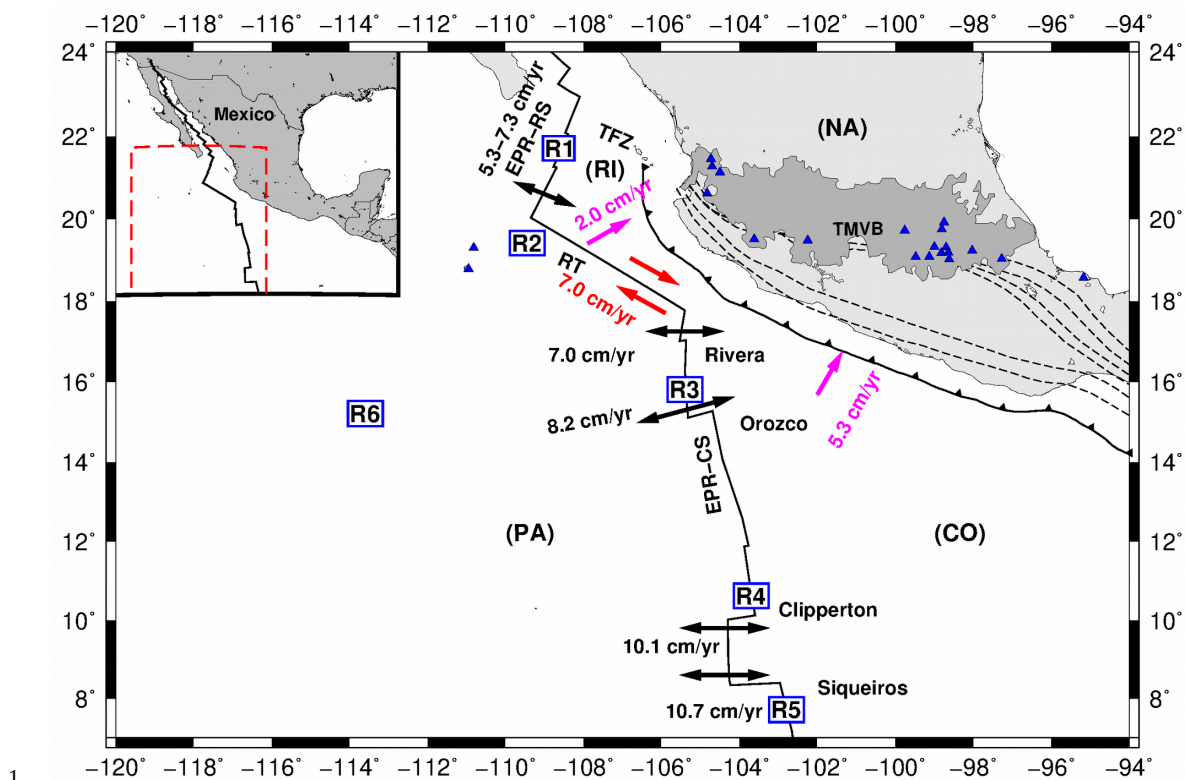
Figure 1

Main tectonic features in the Mexican territory. CO is the Cocos plate, NA is the North American plate,

PA is the Pacific plate, RI is the Rivera microplate, TMVB is the Trans-Mexican Volcanic Belt, TFZ is

the Tamayo fracture zone, EPR-RS is the East Pacific Rise Rivera segment, EPS-CS is the East Pacific

Rise Cocos segment, and RT is the Rivera Transform. Blue triangles are volcanoes. Dashed lines show

contour lines of the subducted slab. Arrows indicate the motion of the PA, CO, and RI plates. R1 to R6

are the regions in which the study are were divided for analyzing stress and seismicity characteristics.

Red number indicates the slipping rates. Pink numbers indicate convergence rates, and black numbers

indicate spreading rates.
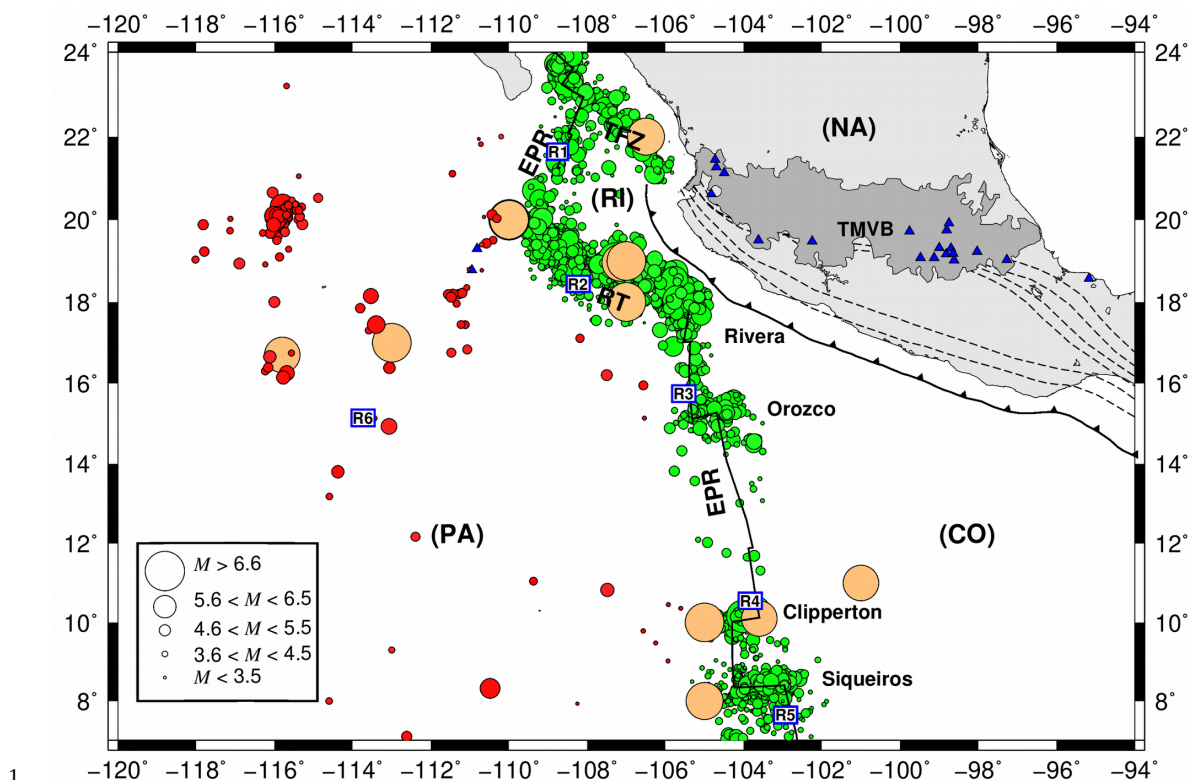
Figure 2

Oceanic seismicity in the Mexico from 1899 to 2017. The size of the circles represents magnitude. Brown circles are relevant historical earthquakes shown in Table 1 with $M > 6.8$. Red circles are intraplate oceanic events, and green circles are transform faults zone, and mid-ocean ridges earthquakes. Epicenters are taken from the Mexican National Service (SSN), and the International Seismological Center (ISC).
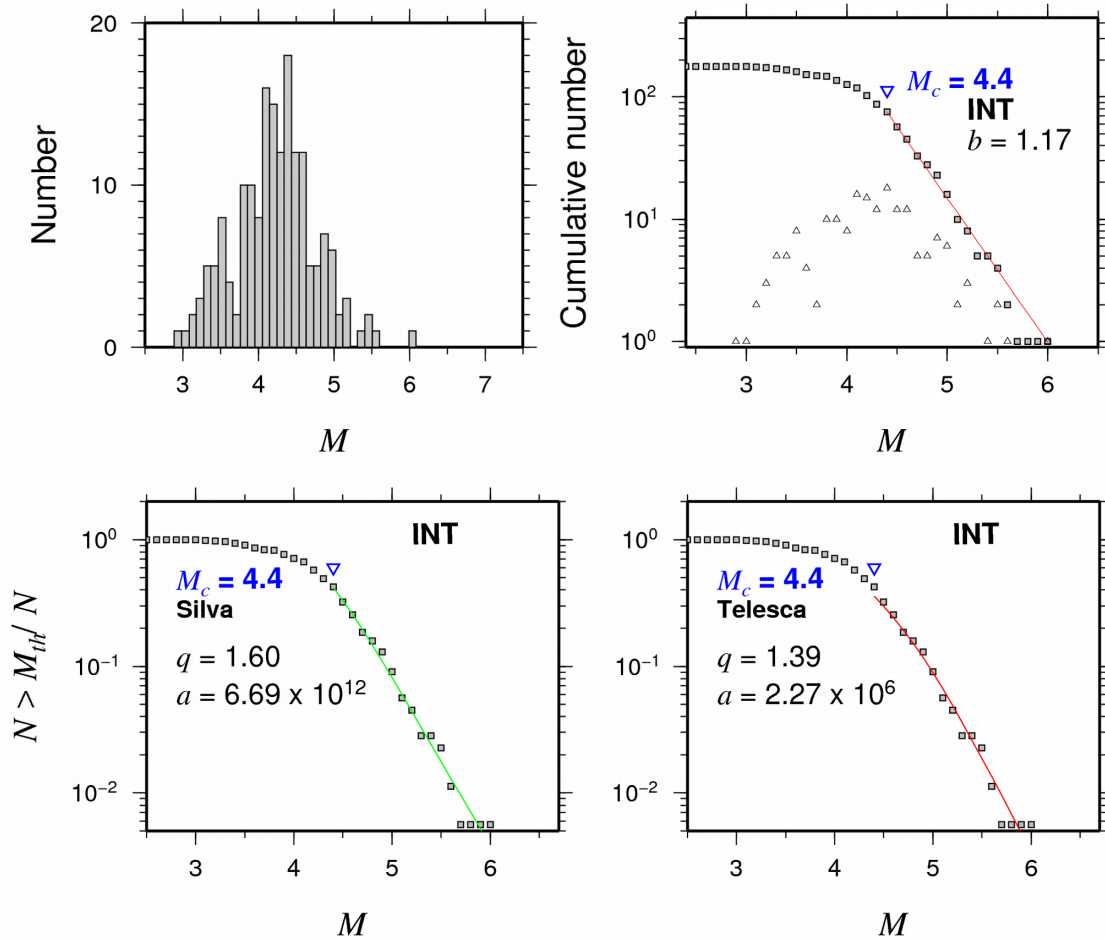
2
3   Figure 3

4   Main statistical characteristics for intraplate oceanic events (INT). Magnitude earthquake histograms

5   (upper left panel); frequency magnitude distributions with M_c, and b-values (upper right panel). The

6   normalized cumulative number of events as function of magnitude for intraplate oceanic events (INT)

7   (lower panels). Color curves show the best fit for the non-extensivity parameters q, and a for the

8   Telesca's (red lines), and the Silva's (green lines) models, respectively.

1 (a)

3 (b)
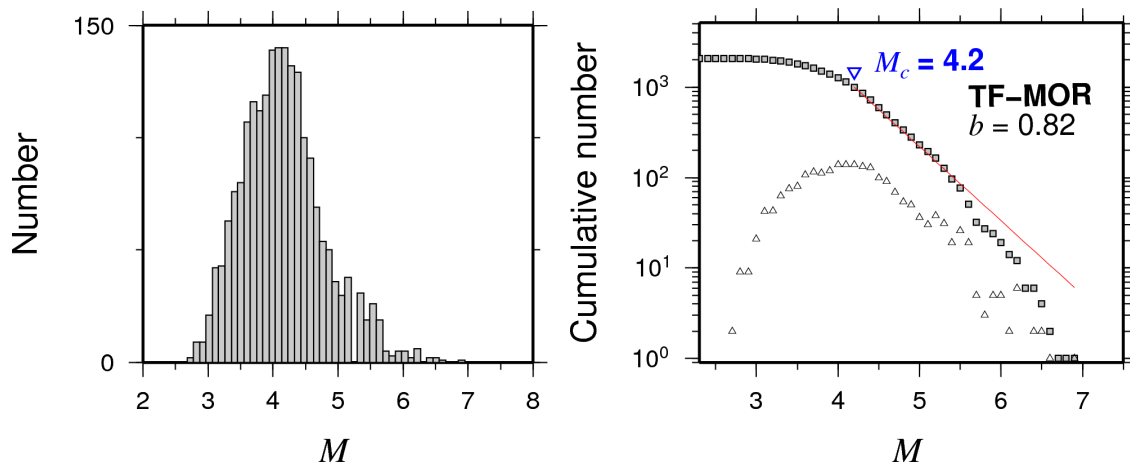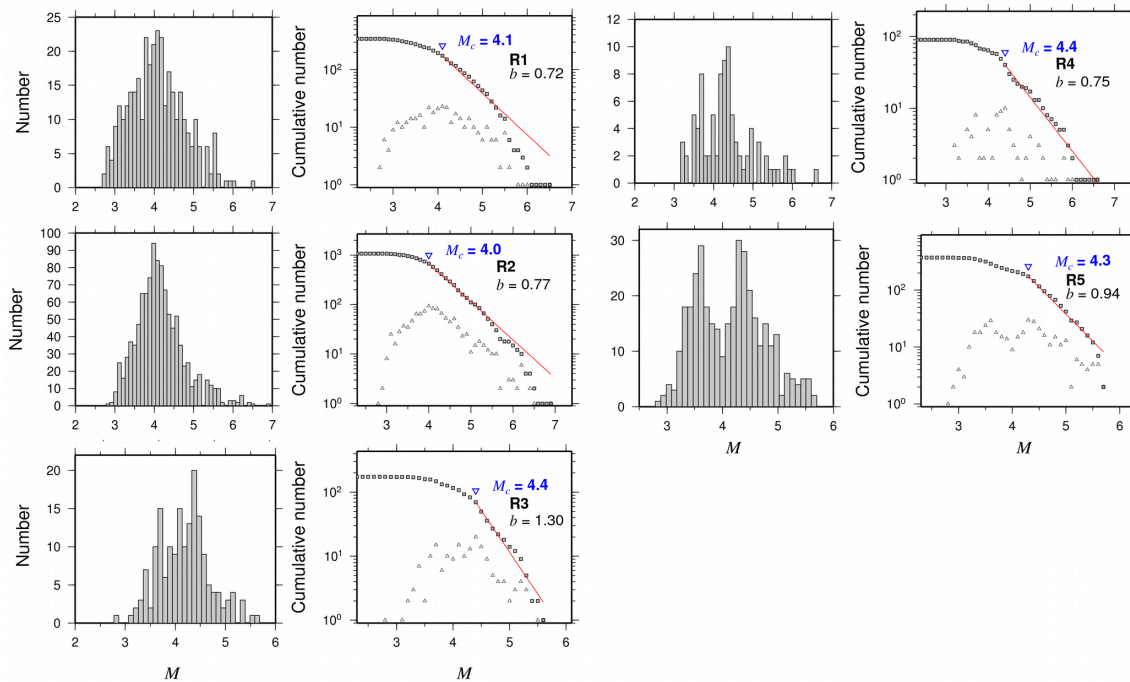
Figure 4

Main statistical characteristics for the transform faults zone, and mid-ocean ridges events (TF-MOR) (regions R1 to R5) (upper panels). Magnitude earthquake histograms, and frequency magnitude distributions with M_c, and b-values for each of the different subregions shown in Fig. 8 (lower panels).
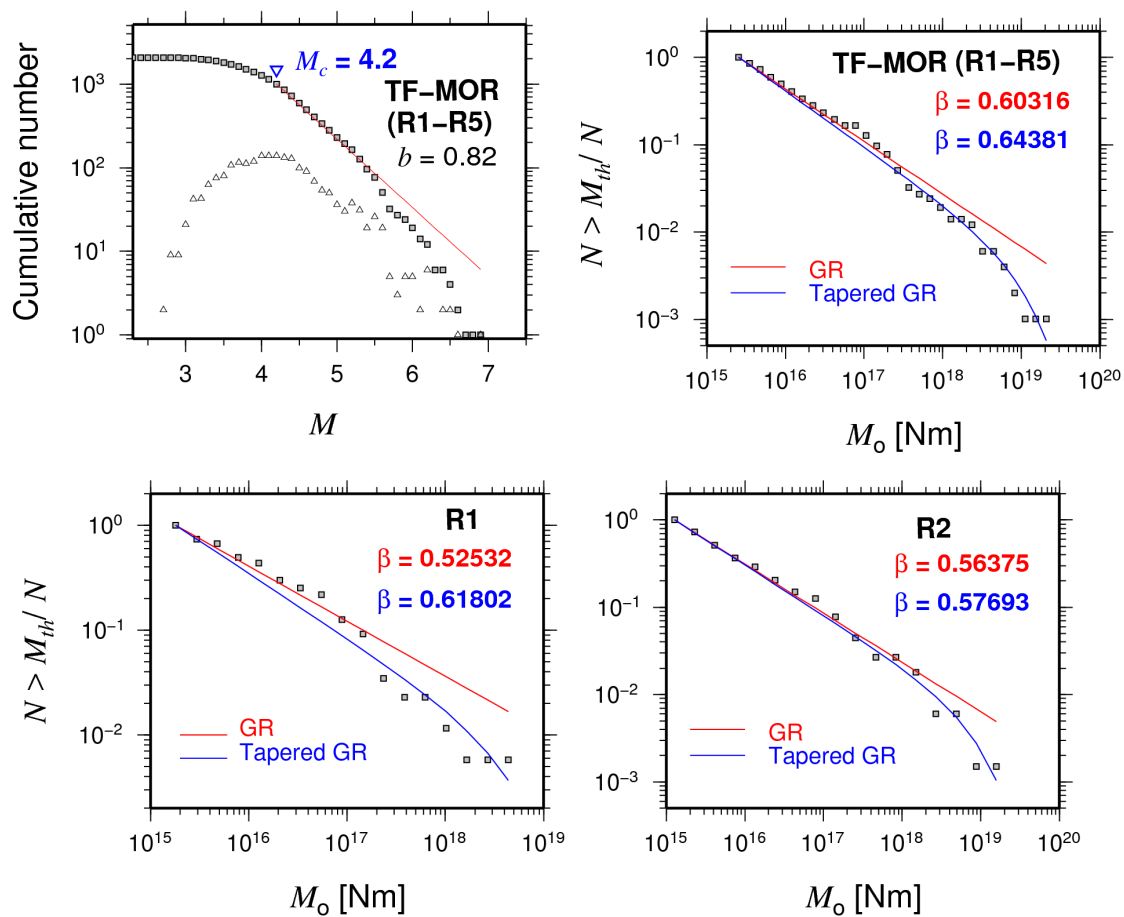
2   Figure 5

3   The cumulative annual seismic moment frequency distribution for the transform faults zone, and mid-

4   ocean ridges events (TF-MOR) (regions R1 to R5) (upper panels). The blue lines are the moment

5   tapered Gutenberg Richter distributions. The red lines represent the ordinary moment Gutenberg

6   Richter distributions. The subregions that do not follow an ordinary moment Gutenberg Richter

7   distribution are subregions R1 and R2 (lower panels).
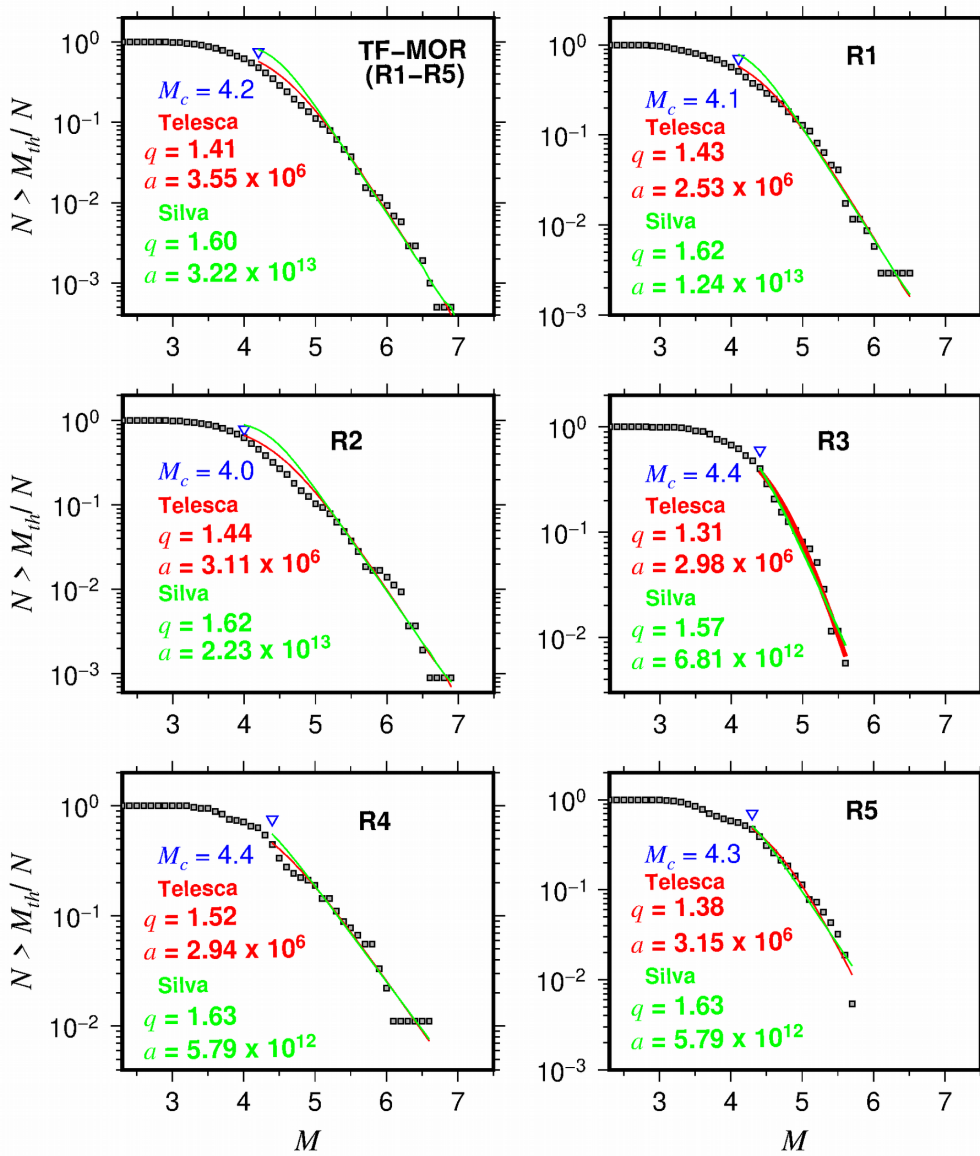
Figure 6

The normalized cumulative number of events as function of magnitude for the transform faults zone,

and mid-ocean ridges events (TF-MOR). Blue triangles show the completeness magnitude (M_c). Red

curves show the best fir for the non-extensivity parameters q, and a for the Telesca's model (red lines).

Green curves show the best fir for the non-extensivity parameters q, and a for the Silva's model (green

lines).

1   (a)

1   (b)
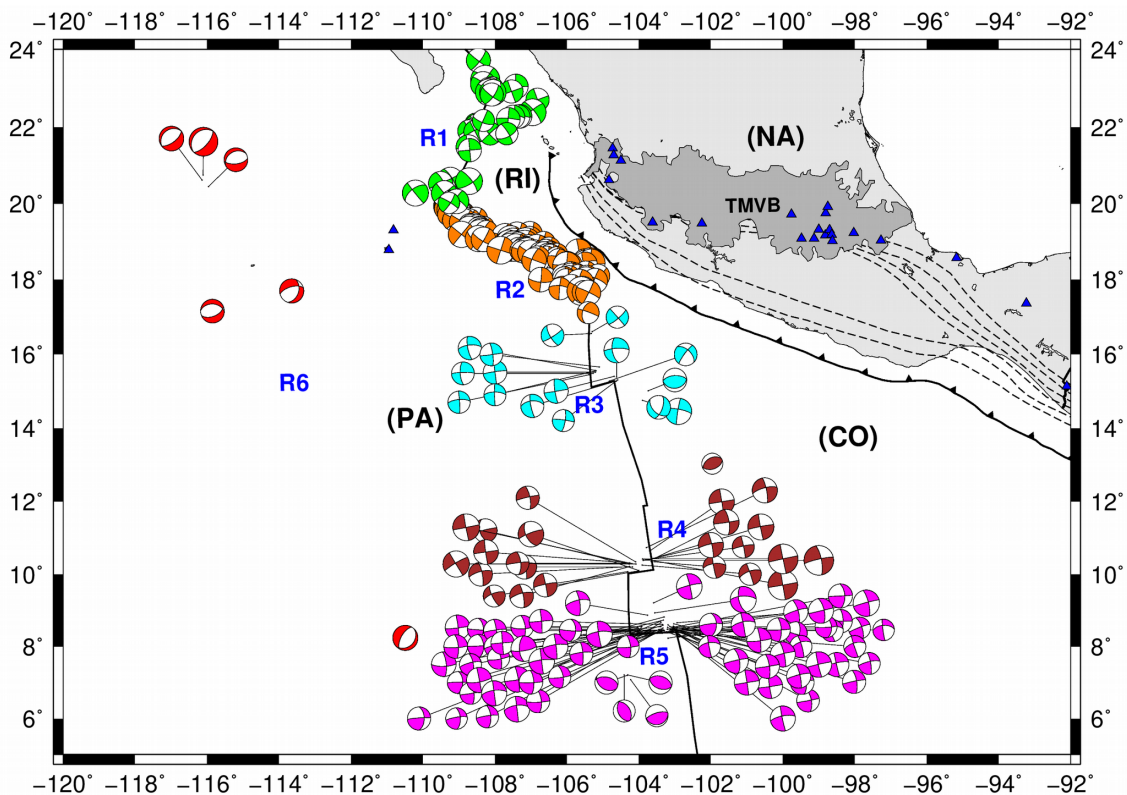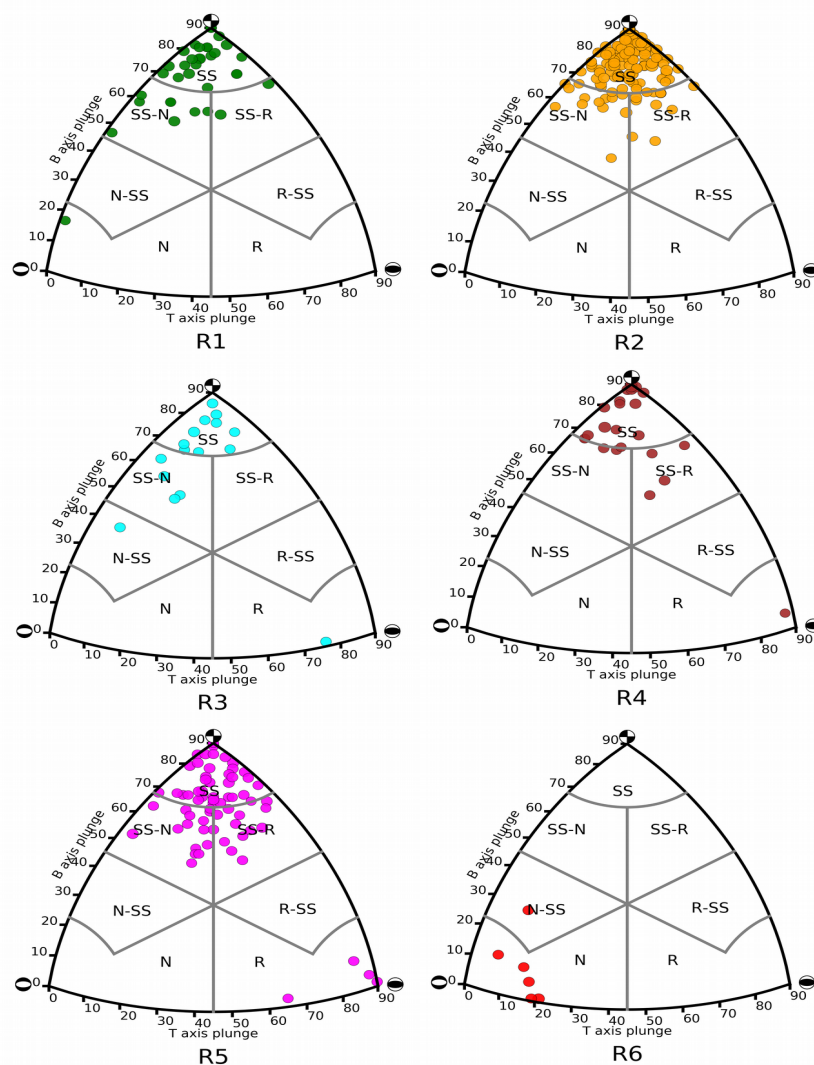
3   Figure 7

4   Focal mechanism solutions of oceanic earthquakes in Mexico reported by the Global CMT catalogue

5   from 1976 to 2017. a) Focal mechanisms are divided into 6 regions (R1 to R6) for the stress inversion

6   analysis. b) Focal mechanism classification based on the Kaverina et al. (1996) projection technique

7   implemented by Álvarez-Gómez (2015): reverse, reverse with lateral component, strike-slip with

8   reverse component, strike-slip, strike-slip with normal component, normal with lateral component, and

9   normal (R, R-SS, SS-R, SS, SS-N, N-SS, and N, respectively).

1 (a)

1 (b)
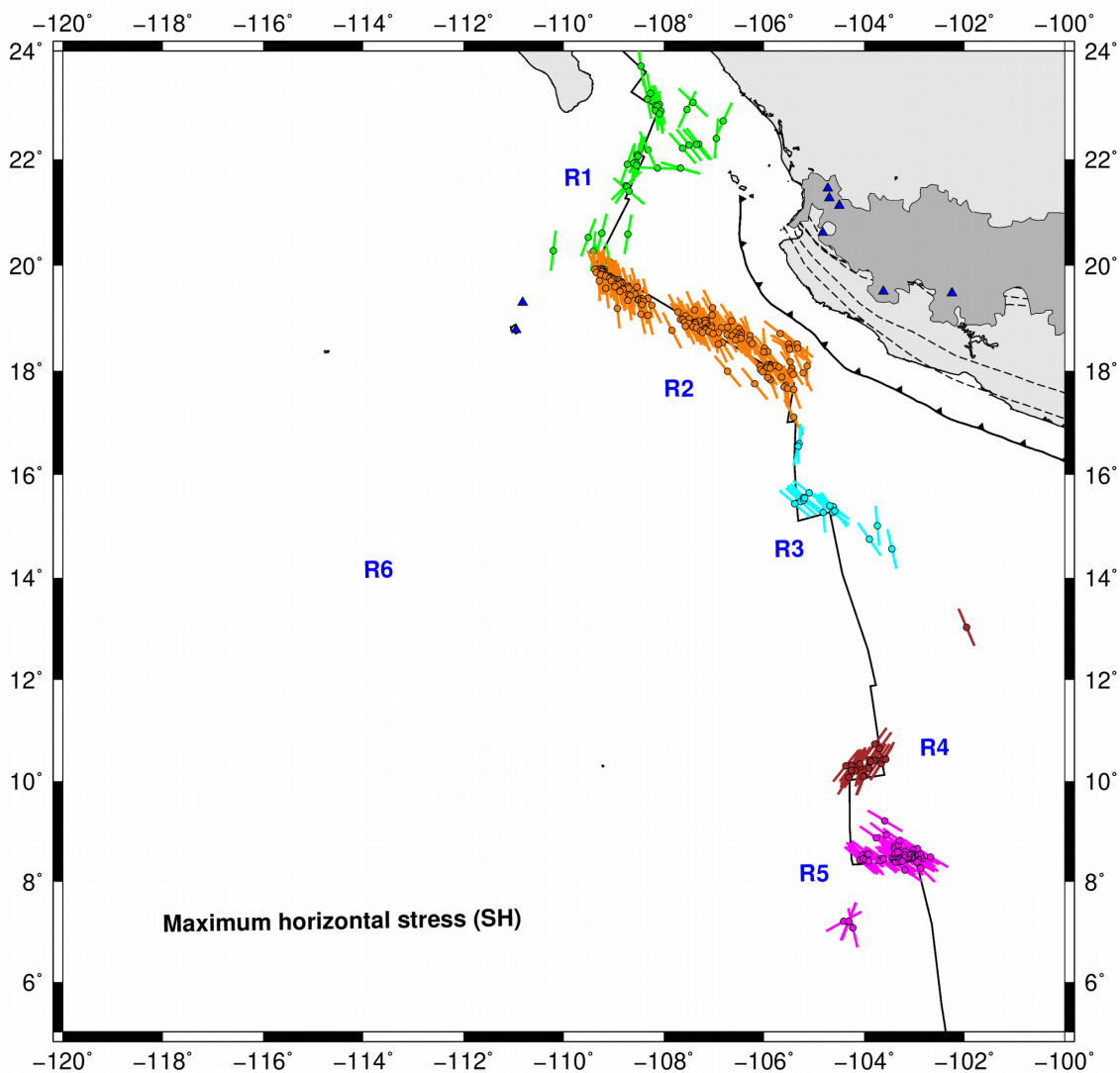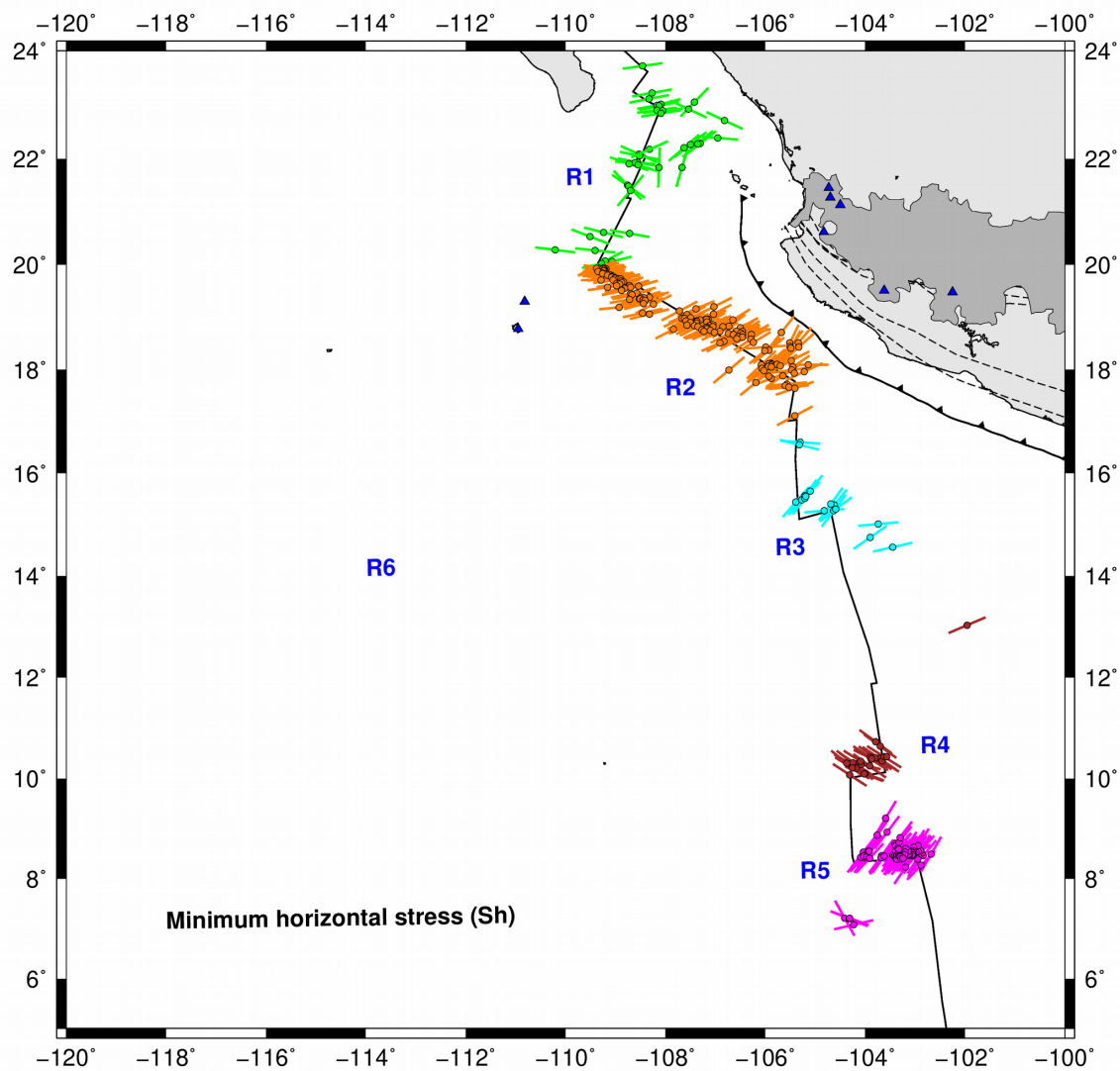
3   Figure 8

4 Orientation of horizontal axes. a) maximum horizontal stresses (SH); b) minimum horizontal stresses

5 (Sh).

1 **Table 1**

2 Major oceanic earthquakes in Mexico ($M > 6.8$)

Event	Date dd/mm/yyyy	Time hh:mm:ss	Lon (°)	Lat (°)	M_s	M_w	M_0	Reference
1	14/01/1899	02:36:00	-110.00	20.00	7.0			1
2	17/12/1905	05:27:00	-113.00	17.00	7.0	7.0	4.40×10^{19}	2
3	10/04/1906	21:18:00	-110.00	20.00	7.1	7.1	6.20×10^{19}	2
4	31/10/1909	10:18:00	-105.00	8.00	6.9			3
5	31/05/1910	04:54:00	-105.00	10.00	7.0			3
6	29/10/1911	18:09:00	-101.00	11.00	6.8			3
7	16/11/1925	11:54:00	-107.00	18.00	7.0			4
8	28/05/1936	18:49:01	-103.60	10.10	6.8			3
9	30/06/1945	05:31:21	-115.80	16.70	6.8			3
10	04/12/1948	04:00:00	-106.50	22.00	6.9			3
11	29/09/1950	06:32:00	-107.00	19.00	7.0			4
12	01/05/1997	11:37:40	-107.15	18.96	6.8	6.9	2.77×10^{19}	5

3 1 Data from the Decade of North American Geology Project (DNA) of the National Geophysical Data

4 Center (NGDC), and the Geological Society of America.

5 2 Pacheco and Sykes (1992)

6 3 ISC earthquake catalog

7 4 Abe (1981)

8 5 Global CMT catalog

12 **Table 2**

13 Statistical parameters

Type	M_c	b-value	q_S-value	a_S-value	q_T-value	a_T-value
INT	4.4	0.89	1.60	6.69×10^{12}	1.39	2.27×10^{6}
TF-MOR (R1- R5)	4.1	0.64	1.60	3.22×10^{13}	1.41	3.55×10^{6}
R1	4.1	0.72	1.62	3.22×10^{13}	1.43	2.53×10^{6}
R2	4.0	0.77	1.62	1.24×10^{13}	1.44	3.11×10^{6}
R3	4.4	1.30	1.57	6.81×10^{12}	1.31	2.98×10^{6}
R4	4.4	0.75	1.70	1.12×10^{13}	1.52	2.94×10^{6}
R5	4.3	0.94	1.63	5.79×10^{12}	1.38	3.15×10^{6}

14 INT are intraplate oceanic events; TF-MOR are transform faults zone, and mid-ocean ridges events; M_c

15 is the completeness magnitude; b is the slope of the Gutenberg-Richter distribution; q_S, a_S, q_T, and a_T

16 are the non-extensive parameters based on Silva et al. (2006), and Telesca (2011), respectively.

1 **Table 3**
2 Aftershocks characteristics of 1 May 1997 event

Date	M_m	M_a	D	p-value	c	k
01/05/1997	6.9	5.3	1.6	0.67 ± 0.33	0.00 ± 0.53	2.12 ± 1.53

3 M_m is the magnitude of the mainshock; M_a is the magnitude of the largest aftershock; D is the
4 difference in magnitudes of the mainshock, and its largest aftershock; p, c, and k are the coefficients of
5 the Omori's law.
6
7
8 **Table 4**
9 Stress inversion results

σ_1 Azimuth/plunge	σ_2 Azimuth/plunge	σ_3 Azimuth/plunge	SH_{max}	R	Region
169°/16°	2°/73°	260°/4°	169	0.37	1[a]
156°/0°	62°/83°	246°/7°	157	0.58	2[a]
157°/4°	31°/84°	247°/5°	157	0.63	3[a]
197°/6°	302°/76°	106°/13°	22	0.84	4[a]
299°/6°	44°/69°	207°/20°	120	0.73	5[a]
247°/80°	39°/9°	130°/5°	45	0.73	6[a]

10 Stress ratio is defined by $R = (\sigma_1 - \sigma_2)/(\sigma_1 - \sigma_3)$; a, stress inversion based on Vavryčuk (2014), and
11 Lund and Townend (2007). Location of the regions are shown in Fig. 1.
12
13
14
15
16
17
18
19
20
21
22
23

Code availability

Generic Mapping Tools (GMT5), Available at: http://gmt.soest.hawaii.edu/, last access: 13 January 2020.

Get_GR_parameters.m, Available at: https://jaolive.weebly.com/codes.html, last access: 23 December 2020.

FMC, Available at: https://josealvarezgomez.wordpress.com/2014/04/22/fmc-a-python-program-to-manage-classify-and-plot-focal-mechanism-data/, last access: 13 January 2020.

Stressinverse_1.1, Available at: https://www.ig.cas.cz/en/stress-inverse/, last access: 13 January 2020.

ZMAP, Available at: http://www.seismo.ethz.ch/en/research-and-teaching/products-software/software/ZMAP/, last access: 13 January 2020.

Data availability

Earthquake catalogs data available at:

Earthquake catalog of the Servico Sismológico Nacional, http://www.ssn.unam.mx/, last access: 13 January 2020.

Earthquake catalog of the International Earthquake Center: http://www.isc.ac.uk/iscbulletin/search/catalogue/, last access: 13 January 2020.

Team list

Q. Rodríguez-Pérez *E-mail*: quetza@geociencias.unam.mx

V.H. Márquez-Ramírez *E-mail*: marvh@geociencias.unam.mx

F.R. Zúñiga *E-mail*: ramon@geociencias.unam.mx

Author contribution

Quetzalcoaltl Rodríguez-Pérez, Víctor Hugo Márquez, and Francisco Ramón Zúñiga designed the idea

and discussed the results. Quetzalcoatl Rodríguez-Pérez developed the methodology and performed the

analyses. Quetzalcoatl Rodríguez-Pérez prepared the manuscript with contributions from all co-authors.

Competing interests

The authors declare that they have no conflict of interest.

Acknowledgments We thank the Mexican National Seismological Service (SSN) for providing us with
the earthquake catalog. Station maintenance, data acquisition, and distribution is thanks to its
personnel. Quetzalcoatl Rodríguez-Pérez was supported by the Mexican National Council for Science
and Technology (CONACYT) (Catedras program- project 1126).

1 **References**

3 Abe, K.: Magnitudes of large shallow earthquakes from 1904 to 1980, Phys. Earth Planet. Int., 27, 72-

4 92, 1981.

6 Abercrombie, R.E., and Ekström, G.: Earthquake slip on oceanic transform faults, Nature, 410, 74-77,

7 2001.

9 Abercrombie, R.E., and Ekström, G.: A reassessment of the rupture characteristics of oceanic transform

10 earthquakes, J. Geophys. Res., 108, B5, 2003.

12 Aki, K.: Maximum likelihood estimate of b in the formula $\log(N) = a - bM$ and its confidence limits, B.

13 Earthq. Res. I. Tokyo, 43, 237-239, 1965.

15 Álvarez-Gómez, J.A.: FMC: A program to manage, classify and plot focal mechanism data. Version

16 1.01, 2015.

18 Antolik, M., Abercrombie, R., Pan J., and Ekström, G: Rupture characteristics of the 2003 M_w 7.6 mid-

19 Indian Ocean earthquake: implications for seismic properties of young oceanic lithosphere, J. Geophys.

20 Res., 111, B04302, 2006.

22 Bandy, W.L.: Geological and geophysical investigation of the Rivera-Cocos plate boundary:

23 implications for plate fragmentation, Ph.D. thesis, Texas A&M University, College Station, 195pp.,

24 1992.

2   Bandy, W.L., Michaud, F., Mortera Gutierrez, C.A., Dyment, J., Bourgois, J., Royer, J.Y., Calmus, T.,

3   Sosson, M., and Ortega-Ramirez, J.: The Mid-Rivera-Transform discordance: morphology and tectonic

4   development, Pure Appl. Geophys., 168, 1391-1413, 2011.

6   Beroza, G.C., and Jordan, T.: Searching for slow and silent earthquakes using free oscillations, J.

7   Geophys. Res., 95, B3, 2485-2510, 1990.

9   Bird, P., Kagan, Y. Y., and Jackson, D. D.: Plate tectonics and earthquake potential of spreading ridges

10   and oceanic transform faults.In S. Stein and J.T. Freymueller (Eds.), Plate Boundary Zones,

11   Geodynamics Series, American Geophysical Union, 203-218, 2002.

13   Boettcher, M.S., and Jordan, T.H.: Seismic behavior of oceanic transform faults, Fall Meeting,

14   American Geophysical Union (AGU), San Francisco, California, December 10-14, S32E-07, 2001.

16   Boettcher, M.S., and Jordan, T.H.: Earthquake scaling relations for mid-ocean ridge transform faults, J.

17   Geophys. Res., 109, B12302, 2004.

19   Boettcher, M.S., Hirth, G., and Evans, B.: Olivine friction at the base of oceanic seismogenic zones, J.

20   Geophys. Res., 112, B01205, 2007.

22   Boettcher, M.S., and McGuire, J.J.: Scaling relations for seismic cycles on mid-ocean ridge transform

23   faults, Geophys. Res. Lett., 36, L21301, 2009.

1   Boettcher, M.S., Wolfson-Schwehr, M.L., Forestall, M., and Jordan, T.H.: Characteristics of oceanic

2   strike-slip earthquakes differ between plate boundary and intraplate settings, Fall Meeting, American

3   Geophysical Union (AGU), San Francisco, California, December 3-7, 7245 Seismology, 2012.

5   Bohnenstiehl, D.R., Tolstoy, M., Dziak, R.P., Fox, C.G., and Smith, D.K.: Aftershock sequences in the

6   mid-ocean ridge environment: an analysis using hydroacoustic data, Tectonophysics, 354, 49-70, 2002.

8   Bohnenstiehl, D.R., Tolstoy, M., and Chapp, E.: Breaking into the plate: A 7.6 M_w fracture-zone

9   earthquake adjacent to the central Indian Ridge, Geophys. Res. Lett., 31, L02615, 2004.

11   Bohnenstiehl, D.R., Waldhauser, F., and Tolstoy, M.: Frequency-magnitude distribution of

12   microearthquakes beneath the 9°50'N region of the East Pacific Rise, October 2003 through April

13   2004, Geochem. Geophys. Geosyst., 9, Q10T03, 2008.

15   Choy, G.L., and Boatwright, J.: Global patterns of radiated seismic energy and apparent stress, J.

16   Geophys. Res., 100, 18205-18226, 1995.

18   Choy, G.L., and McGarr, A.: Strike-slip earthquakes in the oceanic lithosphere: Observations of

19   exceptionally high apparent stress, Geophys. J. Int., 100, 18205-18226, 2002.

21   Cowie, P.A., Scholz, C.H., Edwards, M., and Malinverno, A.: Fault strain and seismic coupling on Mid-

22   Ocean Ridges, J. Geophys. Res., 98, 17911-17920, 1993.

24   Davis, S.D., and Frohlich, C.: Single-link cluster analysis, synthetic earthquake catalogues and

1   aftershock identification, Geophys. J. Int., 104, 289-306, 1991.

3   DeMets , C., Gordon, R.G., Argus, D.F., and Stein, S.: Effect of recent revisions to the geomagnetic

4   reversal time scale on estimate of current plate motions, Geophys. Res. Lett., 21, 2191-2194, 1994.

6   Dziewonski, A.M., Chou, T.A., and Woodhouse, J.H.: Determination of earthquake source parameters

7   from waveform data for studies of global and regional seismicity, J. Geophys. Res., 86, 2825-2852,

8   1981.

10   Ekström, G., Nettles, M., and Dziewonski, A.M.: The global CMT project 2004-2010: centroid-

11   moment tensors for 13,017 earthquakes, Phys. Earth Planet. Int., 200-201, 1-9, 2012.

13   Frohlich, C.: Practical suggestions for assessing rates of seismic-moment release, B. Seismol. Soc.

14   Am., 97, 1158-1166, 2007.

16   Gephart, J.W., and Forsyth, D.W.: An improved method for determining the regional stress tensor using

17   earthquake focal mechanism data: application to the San Fernando earthquake sequence, J. Geophys.

18   Res., 89, 9305-9320, 1984.

20   Goslin, J., et al.: Extent of Azores plume influence on the Mid-Atlantic Ridge north of the hotspot,

21   Geology, 27(11), 991-994, 1999.

23   Goslin, J., Lourenço, N., Dziak, R.P., Bohnenstiehl, D.R., Haxel, J., and Luis, J.: Long-term seismicity

24   of the Reykjanes Ridge (North Atlantic) recorded by a regional hydrophone array, Geophys. J. Int.,

1   162, 516-524, 2005.

3   Gutenberg, B., and Richter, C.F.: Frequency of earthquakes in California, B. Seismol. Soc. Am., 34,

4   185-188, 1944.

6   Houston, H., Anderson, H., Beck., S. L., Zhang, J., and Schwartz, S.: The 1986 Kermadec earthquake

7   and its relation to plate segmentation, Pure Appl. Geophys., 140, 331-364, 1993.

9   Hwang, L.J., and Kanamori, H.: Rupture process of the 1987-1988 Gulf of Alaska earthquake

10   sequence, J. Geophys. Res., 97, 19881-19908, 1992.

12   Ihmlé, P.F., and Jordan, T.H.: Teleseismic search for slow precursors to large earthquakes, Science, 266,

13   1547-1551, 1994.

15   Ishimoto, M., and Iida, K.: Observations of earthquakes registered with the microseismograph

16   constructed recently, B. Earthq. Res. I. Tokyo, 17, 443-478, 1939.

18   Kagan, Y.Y.: Seismic moment-frequency relation for shallow earthquakes: regional comparisons, J.

19   Geophys. Res., 102, 2835-2852, 1997.

21   Kagan, Y.Y.: Universality of the seismic moment-frequency relation, Pure Appl. Geophys., 155, 537-

22   573, 1999.

24   Kagan, Y.Y., and Jackson, D.D.: Probabilistic forecasting of earthquakes, Geophys. J. Int., 143, 438-

1   453, 2000.

3   Kagan, Y.Y., and Schoenberg F.: Estimation of the upper cutoff parameter for the tapered pareto

4   distribution, J. Appl. Probab., 38A, 158-175, 2001.

6   Kagan, Y.Y.: Seismic moment distribution revisited: I. Statistical results, Geophys. J. Int., 148, 520-

7   541, 2002.

9   Kagan, Y.Y.: Earthquake size distribution: power-law with exponent $\beta \equiv 1/2$?, Tectonophysics, 490,

10   103-114, 2010.

12   Kanamori, H., and Stewart, G.S.: Mode of the strain release along the Gibbs fracture zone, Mid-

13   Atlantic Ridge, Phys. Earth Planet. Int., 11, 312-332, 1976.

15   Kaverina, A.N., Lander, A.V., and Prozorov, A.G.: Global creepex distribution and its relation to

16   earthquake-source geometry and tectonic origin, Geophys. J. Int., 125, 249-265, 1996.

18   Kawasaki, I., Kawahara, Y., Takata, I., and Kosugi, I.: Mode of seismic moment release at transform

19   faults, Tectonophysics, 118, 313-327, 1985.

21   Kisslinger, C.: Aftershocks and fault-zone properties, Adv. Geophys., 38, 1-36, 1996.

23   Klein, F.W., Wright, T., and Nakata, J.: Aftershock decay, productivity, and stress rates in Hawaii:

24   indicators of temperature and stress from magma sources, J. Geophys. Res., 111(B7), B07307, 2006.

2   Läderach, Ch.: Seismicity of ultraslow spreading mid-ocean ridges at local, regional and teleseismic

3   scales: A case study of contrasting segments, Ph.D thesis, University of Bremen, 116 pp., 2011.

5   Lund, B., and Townend, J.: Calculating horizontal stress orientations with full or partial knowledge of

6   the tectonic stress tensor, Geophys. J. Int., 270, 1328-1335, 2007.

8   McGuire, J.J., Ihmlé, P.F., and Jordan, T.H.: Time-domain observations of a slow precursor to the 1994

9   Romanche transform earthquake, Science, 274, 82-85, 1996.

11 McGuire, J.J., Boettcher M.S., and Jordan, T.H.: Foreshock sequences and short-term earthquake

12 predictability on East Pacific Rise transform faults, Nature, 434, 457-461, 2005.

14 McGuire, J.J.: Seismic cycles and earthquake predictability on East Pacific Rise transform faults, B.

15 Seismol. Soc. Am., 98, 1067-1084, 2008.

17 McGuire, J.J., Collins, J.A., Gouédard, P., Roland, E., and Lizarralde, D.: Variations in earthquake

18 rupture properties along the Gofar transform fault, East Pacific Rise, Nat. Geosci., 5, 336-341, 2012.

20 Mogi, K.: Magnitude-frequency relation for elastic shocks accompanying fractures of various materials

21 and some related problems in earthquakes, B. Earthq. Res. I. Tokyo, 40, 831-853, 1962.

23 Molchan, G., Kronrod, T., and Panza, G.F.: Multi-scale seismicity model for seismic risk, B. Seismol.

24 Soc. Am., 87, 1220-1229, 1997.

2   Nelder, J.A., and Mead, R.: A simplex method for function minimization, Comput. J., 7, 308-313, 1965.

4   Nuannin, P., Kulhanek, O., and Persson, L.: Variations of *b*-value preceding large earthquakes in the

5   Andaman-Sumatra subduction zone, J. Asian Earth Sci., 61, 237-242, 2012.

7   Okal, E.A., and Stewart, L.M.: Slow earthquakes along oceanic fracture zones: evidence for

8   asthenospheric flow away from hotspots?, Earth Planet. Sci. Lett., 57, 75-87, 1992.

10   Olive, J-A.: Get_GR_parameters.m Matlab function for analysis of earthquake catalogs. Available at:

11   https://jaolive.weebly.com/codes.html, 2016.

13   Pacheco, J.F., and Sykes, L.R.: Seismic moment catalog of large shallow earthquakes, 1900 to 1989, B.

14   Seismol. Soc. Am., 82, 1306-1349, 1992.

16   Papadakis, G., Vallianatos, F., and Sammonds, P.: Evidence of nonextensive statistical physics behavior

17   of the Hellenic subduction zone seismicity, Tectonophysics, 608, 1037-1048, 2013.

19   Pockalny, R.A., Fox, P.J., Fornari, D.J., McDonald, K., and Perfit, M.R.: Tectonic reconstruction of the

20   Clipperton and Siqueiros Fracture zones: evidence and consequences of plate motion change for the

21   last 3Myr, J. Geophys. Res., 102, 3167-3181, 1997.

23   Rabinowitz, N., and Steinberg, D.M.: Aftershock decay of the three recent strong earthquakes in the

24   Levant, B. Seismol. Soc. Am., 88, 1580-1587, 1998.

2 Riedesel, M., Orcutt, J.A., McDonald, K.C., and McClain, J.S.: Microearthquakes in the Black Smoker

3 Hydrothermal Field, east Pacific Rise at 21º N, J. Geophys. Res., 87, 10613-10623, 1982.

5 Rodríguez-Pérez, Q, and Zúñiga, F. R.: Seismicity characterization of the Maravatío-Acambay and

6 Actopan regions, central Mexico, J. S. Am. Earth Sci., 76, 264-275, 2017.

8 Rodríguez-Pérez, Q, and Zúñiga, F. R.: Imaging b-value depth variations within the Cocos and Rivera

9 plates at the Mexican subduction zone, Tectonophysics, 734, 33-43, 2018.

11 Roland, E., Behn, M.D., and Hirth, G.: Thermal-mechanical behavior of oceanic transform faults:

12 Implications for the spatial distribution of seismicity, Geochem. Geophys. Geosyst., 11, Q07001, 2010.

14 Scholz, C.H.: The frequency-magnitude relation of micro fracturing in rock and its relation to

15 earthquakes, B. Seismol. Soc. Am., 58, 388-415, 1968.

17 Schorlemmer, D.S., Wiemer, S., and Wyss, M.: Variations in earthquake-size distribution across

18 different stress regimes, Nature, 437, 539-542, 2005.

20 Scordilis, E.M.: Empirical global converting M_s and m_b to moment magnitude, J. Seismol., 10, 225-

21 236, 2006.

23 Shcherbakov, R., Turcotte, D.L., and Rundle, J.B.: A generalized Omoris's law for earthquakes

24 aftershocks decay, Geophys. Res. Lett., 31(11), L11613, 2004.

2 Silva, R., Franca, G., Vilar, C., and Alcaniz, J.: Nonextensive models for earthquakes, Phys. Rev. E, 73,

3 026102, 2006.

5 Smith, W.D.: The *b*-value as an earthquake precursor, Nature, 289, 136-139, 1981.

7 Smith, D.K., Tolstoy, M., Fox, C.G., Bohnenstiehl, D.R., Matsumoto, H., and Fowler, M.J.:

8 Hydroacoustic monitoring of seismicity at the slow-spreading Mid-Atlantic Ridge, Geophys. Res. Lett.,

9 29(11), 2002.

11 Smith, D.K., Escartin, J., Cannat, M., Tolstoy, M., Fox, C.G., Bohnenstiehl, D.R., and Bazin, S.: Spatial

12 and temporal distribution of seismicity along the northern Mid-Atlantic Ridge (15°-35°), J. Geophys.

13 Res., 108(B3), 2003.

15 Simão, N., Escartín, J., Goslin, J., Haxel, J., Cannat, M., and Dziak, R.: Regional seismicity of the Mid-

16 Atlantic Ridge: observations from autonomous hydrophone arrays, Geophys. J. Int., 183, 1559-1578,

17 2010.

19 Sotolongo-Costa, O., and Posadas, M.A.: Fragment-asperity interaction model for earthquakes, Phys.

20 Rev. Lett., 92, 048501, 2004.

22 Stein, S., and Pelayo, A.: Seismological constraints on stress in the oceanic lithosphere, Philosophical

23 Transactions of the Royal Society of London A, 337, 53-72, 1991.

1   Sykes, L.R.: Mechanism of earthquakes and nature of faulting on the mid-oceanic ridges, J. Geophys.

2   Res., 72, 2131-2153, 1967.

4   Telesca, L.: Nonextensive analysis of seismic sequences, *Physica A*, 389, 1911-1914, 2009.

6   Telesca, L.: A non-extensive approach in investigating the seismicity of L'Aquila area (central Italy),

7   struck by the 6 April 2009 earthquake (M_L = 5.8), Terra Nova, 22, 87-93, 2010.

9   Telesca, L.: Tsallis-based nonextensive analysis of the Southern California seismicity, Entropy, 13,

10   1267-1280, 2011.

12   Tolstoy, M., Bohnenstiehl, D.R., and Edwards, M.H.: Seismic character of volcanic activity at the

13   ultraslow-spreading Gakkel Ridge, Geology, 29, 1139-1142, 2001.

15   Tsallis, C.: Possible generalization of Boltzmann-Gibbs statistics, J. Stat. Phys., 52, 479-487, 1988.

17   Urbancic, T.I., Trifu, C.I., Long, J.M., and Young, R.P.: Space-time correlation of *b*-values with stress

18   release, Pure Appl. Geophys., 139, 449-462, 1992.

20   Utsu, T.: A statistical study on the occurrence of aftershocks, Geophysical Magazine, 30, 521-605,

21   1961.

23   Utsu, T., Ogata, Y., and Matsura, R.S.: The centenary of the Omori formula for a decay law of

24   aftershock activity, J. Phys. Earth., 43, 1-33, 1995.

2 Utsu, T.: Statistical features of seismicity, International Handbook of Earthquake and Engineering

3 Seismology, Part A. Academic Press, pp. 719-732, 2002.

5 Valverde-Esparza, S.M., Ramirez-Rojas, A., Flores-Marquez, E.L., and Telesca, L.: Non-extensivity

6 analysis of seismicity within four subduction regions in Mexico, Acta Geophys., 60, 833–845, 2012.

8 Vavryčuk, V.: Iterative joint inversion for stress and fault orientations from focal mechanisms,

9 Geophys. J. Int., 199, 69-77, 2014.

11 Velasco, A.A., Ammon, C.J., and Beck, S.L.: Broadband source modeling of the November 8, 1997,

12 Tibet (M_w = 7.5) earthquake and its tectonic implications, J. Geophys. Res., 105(B12), 28065-28080,

13 2000.

15 Vere-Jones, D., Robinson, R., and Yang, W.Z.: Remarks on the accelerated moment release model:

16 problems of model formulation, simulation and estimation, Geophys. J. Int., 144, 517-531, 2001.

18 Vilar, C.S., Franca, G., Silva, R., and Alcaniz, J.S.: Nonextensivity in geological faults?, Physica A,

19 377, 285-290, 2007.

21 Vallianatos, F.: A non-extensive approach to risk assessment, Nat. Hazards Earth Syst. Sci., 9, 211-216,

22 2009.

24 Warren, N.W., and Latham, G.V.: An experimental study of the thermally induced microfracturing and

1   its relation to volcanic seismicity, J. Geophys. Res., 75, 4455-4464, 1970.

3   Wesnousky, S.G.: The Gutenberg-Richter or characteristic earthquake distribution, which is it?, B.

4   Seismol. Soc. Am., 84, 1940-1959, 1994.

6   Wiens, D.A., and Stein, S.: Intraplate seismicity and stresses in young oceanic lithosphere, J. Geophys.

7   Res., 89, 11442-11464., 1984.

9   Wiemer, S., and Benoit, J.P.: Mapping the *b*-value anomaly at 100 km depth in the Alaska and New

10   Zealand subduction zones, Geophys. Res. Lett., 23, 1557-1560, 1996.

12   Wiemer, S., and Wyss, M.: Minimum magnitude of completeness in earthquake catalogues: Examples

13   from Alaska, the western United States, and Japan, B. Seismol. Soc. Am., 90, 859-869, 2000.

15   Wiemer, S.: A software package to analyze seismicity: ZMAP, Seismol. Res. Lett., 72, 373-382, 2001.

17   Wolfe, C.J., Bergman, E.A., and Solomon, S.C.: Oceanic transform earthquakes with unusual

18   mechanisms or locations: relation to fault geometry and state of stress in the adjacent lithosphere, J.

19   Geophys. Res., 98, B9, 16187-16211, 1993.

21   Wolfson-Schwehr, M., Boettcher, M.S., McGuire, J.J., and Collins, J.A.: The relationship between

22   seismicity and fault structure on the Discovery transform fault, East Pacific Rise, Geochem. Geophys.

23   Geosyst., 15, 3698-3712, 2014.

1   Wyss, M.: Towards a physical understanding of the earthquake frequency distribution, Geophys. J. Roy.

2   Astron. Soc., 31, 341-359, 1973.